RSC Advances

This article can be cited before page numbers have been issued, to do this please use: Y. Liu, H. Zhong, Y. Qin, Y. Zhang, X. Liu and T. Zhang, *RSC Adv.*, 2016, DOI: 10.1039/C6RA04349F.

ROYAL SOCIETY OF CHEMISTRY

www.rsc.org/advances

View Article Online
DOI: 10.1039/C6RA04349F

Non-covalent hydrophilization of reduced graphene oxide used as paclitaxel vehicle

Yu Liu[1], Han Zhong[1], Yu Qin[1], Yan Zhang[1,2], Xinfeng Liu[3], Tao Zhang[1,2,*]

1. College of Engineering and Applied Sciences, Nanjing University, Nanjing 210093, China

2. Nanjing Excellence Technology Center for Interventional Medical Devices, Nanjing 210093, China

3. Department of Neurology, Jinling Hospital, Nanjing University School of Medicine, Nanjing 210003, China

Abstract

Graphene oxide (GO) and reduced graphene oxide (RGO) are attractive materials due to their potential biomedical applications, especially as drug delivery vehicles because of their huge specific surface area. In the current study, GO and RGO were prepared. In addition, a perylene derivative, phosphorylcholine oligomer grafted perylene (Perylene-PCn), was synthesized following the atom transfer radical polymerization procedure. In order to determine their structures, the products were characterized carefully with Fourier transform infrared spectra, proton nuclear magnetic resonance, X-ray photoelectron spectroscopy, wide angel X-ray diffraction, thermogravimetric analysis, and atomic force microscope etc. The properties including fluorescence and biocompatibility were also evaluated. Utilizing the

* To whom correspondence should be addressed. E-mail: ztnj@nju.edu.cn

View Article Online
DOI: 10.1039/C6RA04349F

π-π stacking interaction of RGO and perylene moiety, a water dispersible RGO/Perylene-PCn composites were fabricated and then investigated as a vehicle of anti-tumor paclitaxel (PTX). The anti-tumor effects of free PTX and PTX@RGO/Perylene-PCn were compared with an *in vitro* cytotoxicity assay. The results demonstrate that RGO/Perylene-PCn can be used as an anti-tumor agent delivery vehicle for potential oncology applications.

Introduction

Since firstly reported in 2004, graphene has drawn a great deal of attentions due to its extraordinary electrical, optical, catalytic and mechanical properties [1-4]. Graphene is consisted of layers of π-conjugated structures of six-carbon rings, which can be conceptually viewed as a planar aromatic macromolecule. This planar structure offers an excellent capability of immobilizing a large number of substances, including metals, drugs, biomolecules, fluorescent probes and cells [5-10]. Therefore, it is not surprising that graphene have been extensively investigated for its nanomedicine and biomedical applications, including but not limited to drug delivery platform for anti-cancer/gene delivery, biosensing, bioimaging, antibacterial applications, cell culturing and tissue engineering [6, 7, 9-13].

However, the applications of graphene were limited due to the insolubility of graphene in water and the tendency of agglomerating irreversibly or even restacking into graphite through Van der Waals interactions [14]. Thus, the modifications of graphene turned out to be of great importance for their potential biomedical applications. Usually, there are two methods to prepare the soluble graphene, namely chemical modifications and non-covalent

View Article Online
DOI: 10.1039/C6RA04349F

functionalization. The chemical modification, which usually means covalent modifications on graphene, may result in the changes of their electronic structure by creating sp^3 centers, leading to the alteration of its physical properties [15-17]. On the other hand, it was believed that the non-covalent functionalization, which mainly relies on Van der Waals interactions or π-π stacking interactions, normally impacted little on structures and properties of graphene. Stankovich et al. reported the first example of non-covalent functionalization of graphitic nanoplatelets using poly(sodium 4-styrenesulphonate) [18]. Liu et al. designed a series of pyrene terminated polymers to functionalize reduced graphene oxide (RGO) via π-π stacking interaction [19, 20]. Feng et al. functionalized graphene oxide (GO) by PEI polymers utilizing non-covalent electrostatic interactions, which produced GO-PEI complexes with strong positive charges, high stability in physiological solutions and reduced cytotoxicity to cells [21]. Yang et al. constructed a nanosuperamolecular assembly using folic acid-modified β-cyclodextrin and GO non-covalently, which were linked by an adamantane-grafted porphyrin through π-π stacking interaction [22]. Depan et al. prepared a novel folate-decorated and graphene-mediated drug delivery system by attaching doxorubicin to GO via strong π-π stacking interaction, followed by encapsulation of GO with folic acid conjugated chitosan to enhance the stability of the nano-carrier system in aqueous medium [23].

In this work, perylene-3,4,9,10-tetracarboxylic acid bisimide (PBI) connected with phosphorylcholine oligomers has been employed to modify graphene by π-π stacking interaction. PBI derivatives are highly fluorescent, chemically and photochemically stable molecules which have been used as pigments and dyes. In previous work, Kang et al. designed perylene containing poly(glyceryl acrylate) derivatives to modify reduced graphene

View Article Online
DOI: 10.1039/C6RA04349F

oxide. The low cytotoxicity of the hybrids was shown by treating 3T3 fibroblasts with the hybrids *in vitro* [24]. Phospholipids are components of lipid bilayers and plasma membranes [25]. It is believed that polymers containing a phospholipid structure are highly biocompatible as a result of their characteristic ability to mimic biomembranes [26]; however, phospholipid molecules cannot bond covalently and, as a result, are highly mobile. A simple bilayer membrane containing a phospholipid structure cannot provide the physical and chemical properties necessary to maintain stability [27]. To obtain stable phospholipid systems, several phospholipid-analogous molecules with polymerizable groups have been synthesized [28]. Among them, 2-methacryloyloxyethyl phosphorylcholine (MPC) is one of the most effective compounds. It has been proven to be capable of significantly reducing protein absorption as well as platelet and cell adhesion to materials [29-31]. Soon after its debut, MPCs have been introduced into many materials by grafting onto a functionalized surface to enhance the material's biocompatibility [32-34].

Initially, Perylene-PCn was synthesized with atom transfer radical polymerization (ATRP) method from MPC as monomer and PBI derivative as an initiator. Graphene, or more accurately, the reduced graphene oxide (RGO), was obtained from chemical reduction of GO by $N_2H_2 \cdot H_2O$. Then, Perylene-PCn was allowed to self-assemble onto the RGO nanosheets via π-π stacking interactions to achieve non-covalent functionalization of graphene. In the present study, paclitaxel loading RGO/PBI-PCn were fabricated by self-attachment in ethanol solution at room temperature with ultrasonication. Paclitaxel (PTX) is one of the most widely used anticancer agents, that shows activities against various solid tumors [35]. The current study outlines the characterizations of RGO/PBI-PCn, *in vitro* toxicity of paclitaxel loading

View Article Online
DOI: 10.1039/C6RA04349F

RGO/PBI-PCn against L929 murine fibroblasts and human gastric cell lines SGC-7901.

Experimental

Materials

The natural graphite powder (C > 99% with particle size about 5 μm) was purchased from Shanghai Huayuan Graphite Co., Ltd. (Shanghai, China). $KMnO_4$, H_2SO_4 (98%), H_2O_2 (30% solution in water) and Hydrazine hydrate ($N_2H_4 \cdot H_20$, 80%) were purchased from Nanjing Reagent Co. Ltd. (Nanjing, China). N,N,N',N",N''-Pentamethyldiethylenetriamine (PMDETA, 99%), CuBr (99%), 2-Bromoisobutyryl bromide (99%) and Perylene-3,4,9,10-tatracarboxylic dianhydride (PTCDA) were purchased from Aladdin Chemistry Co. Ltd. (Shanghai, China). Inhibitor-free 2-Methacryloyloxyenthyl Phosphorylcholine (MPC, > 96%) was supplied by Joy-Nature Institute of Technology (Nanjing, China). Paclitaxel (PTX) were offered by Jiangsu Yew Pharmaceutical Co., Ltd. (Jiangsu, China). All other reagents and solvents were purchased from Aladdin Chemistry Co. Ltd. (Shanghai, China) and used as received.

Human umbilical vein endothelial cell lines (HUVEC), mouse leukaemic monocyte macrophage cell lines (RAW264.7), mouse fibroblast cell lines (L929) and human gastric cancer cell lines (SGC-7901) were obtained from Zhongyuan Co., Ltd (Beijing, China). Dulbecco's modified Eagle's medium (DMEM, with 4500 mg/L-glucose and L-glutamine) was purchased from Thermo Fisher Scientific Inc. (Beijing, China). Fetal bovine serum (FBS) was purchased from Hangzhou Sijiqing Biological Engineering Materials Co., Ltd. (Hangzhou, China), which was heat inactivated for 30 min at 56°C and then stored at -20°C before use. 0.25% trypsin-EDTA (1X) with phenol red was purchased from Life Technologies Co.

View Article Online
DOI: 10.1039/C6RA04349F

(Shanghai, China). Penicillin/streptomycin (100×) was purchased from Life Technologies Co. (Shanghai, China). Cell Counting Kit-8 (CCK-8) was obtained from Dojindo Molecular Technologies, Inc. (Shanghai, China).

Instruments

Proton nuclear magnetic resonance (^{1}H-NMR) spectra were recorded on a Bruker ARX500 NMR Spectrometer (Bruker, German) using D_2O as the solvent. Fourier transform infrared spectra (FTIR) were recorded on a PE GX spectrometer (Perkin-Elmer, USA) at room temperature on KBr pellets with sample concentrations of ~1% from 4000 to 400 cm^{-1} with a resolution of 4 cm^{-1}. Thermogravimetric Analysis (TGA) were recorded on a Netzsch STA409PC (Selb, Germany) in N_2 atmosphere at the heating rate 20 °C·min^{-1} from room temperature to 700 °C. Wide angle X-ray diffraction (XRD) measurements were performed on a Rigaku ULTIMA-3 setup with Mar 345 image plate as detector and the Cu Kα was used as the source (wavelength = 0.1542 nm). The recorded region of 2θ was from 3° to 45° with scanning speed 2°·min^{-1}. A tapping mode atomic force microscope (AFM) (NanoScope IIIa, Digital Instrument, Inc.) was utilized to observe the micromorphology of samples. A LabRAM Aramis Raman Spectrometer (LabRAM HORIBA Jobin Yvon, Edison, NJ, USA) excited by the 532 nm coherent line of a Nd:YAG laser was used to determine the carbon structure of the samples at room temperature, the samples were prepared by casting suspensions onto the silicon substrates and drying at 60 °C for 24 h. X-ray Photoelectron Spectroscopy (XPS) measurements were recorded on a Thermo Scientific K-Alpha Photoelectron Spectrometer equipped with a monochromatic Al Kα X-ray source. XPS PEAK software (v4.1) was utilized to analyze and deconvolute the XPS peaks. Peak deconvolutions were performed using optional

View Article Online
DOI: 10.1039/C6RA04349F

Lorentzian-Gaussian components after a Shirley background subtraction. The Ultraviolet-visible absorption spectra were obtained from a MAPADA UV-1800PC spectrophotometer (Shanghai, China). Fluorescence experiments were carried out on a Horiba Fluorolog-3-22 spectrofluorometer (Horiba Scientific, Japan) with 373 nm excitation wavelength (20 nm band pass for both entrance and exit). The cells used in the cytotoxicity evaluations were cultivated in a Heracell model 150i CO_2 incubator (Thermo Scientific, USA), and the evaluations were carried out with an RT-6000 micro-plate reader (Rayto Ltd., Shenzhen, China) at a wavelength of 450 nm. The confocal fluorescent images were taken with an Olympus Fluoview confocal microscope (Olympus, Japan).

Preparation of GO and RGO

GO was prepared from natural graphite powder according to the modified Hummers method [36]. In detail, 2 g graphite powders were added into 50 mL cooled (0 °C), stirring concentrated H_2SO_4. Then, 6 g $KMnO_4$ was charged gradually below 5 °C. After being stirred below 5 °C for 1 h, the mixture was heated to 35 °C and kept stirring for 30 min. In order to dilute the reaction system, 100 mL distilled water was dropped slowly and the temperature was maintained no more than 100 °C. At last, 15 mL 30% H_2O_2 was added. The crude GO was filtered off, washed with 5% HCl solution and distilled water for at least 3 times, and then dialyzed for at least 48 h until SO_4^{2-} could not be determined by $BaCl_2$ solution. GO was filtered out again and vacuum dried under 60 °C to obtain the dried target products.

In a 250 mL round bottom flask, 100 mg GO and 100 mL water were added to obtain an inhomogeneous yellow-brown dispersion. The dispersion was ultrasonicated till clear

View Article Online
DOI: 10.1039/C6RA04349F

without any visible particles. 3 mL hydrazine hydrate was then added and the solution was heated in an oil bath at 90 °C for 24h, over which the RGO gradually precipitated out as a black solid[37, 38]. The products were isolated by filtration over a medium fritted glass funnel, washed copiously with water, and dried on the funnel at 60 °C over night.

Synthesis of Perylene-PCn

Perylene-PCn was synthesized via ATRP, with PBI derivative as initiator and MPC as monomer in 3 steps illustrated in Figure 1.

Step 1. Preparation of PBI-OH: PTCDA (400 mg, 1 mmol) and ethanol amine (7.92 g, 40 mmol) were introduced into a 50 mL Teflon lining hydro-thermal reaction kettle. The mixture was ultrasonicated for 10 min and sealed, reacted at 150 °C for 24 h. The unreacted ethanol amine was removed by filtration, washing with copious amount of water and vacuum drying. N,N'-bis(oxethyl)perylene-3,4,9,10-tetracarboxylic acid bisimide (PBI-OH) was obtained as a dark red solid [39, 40].

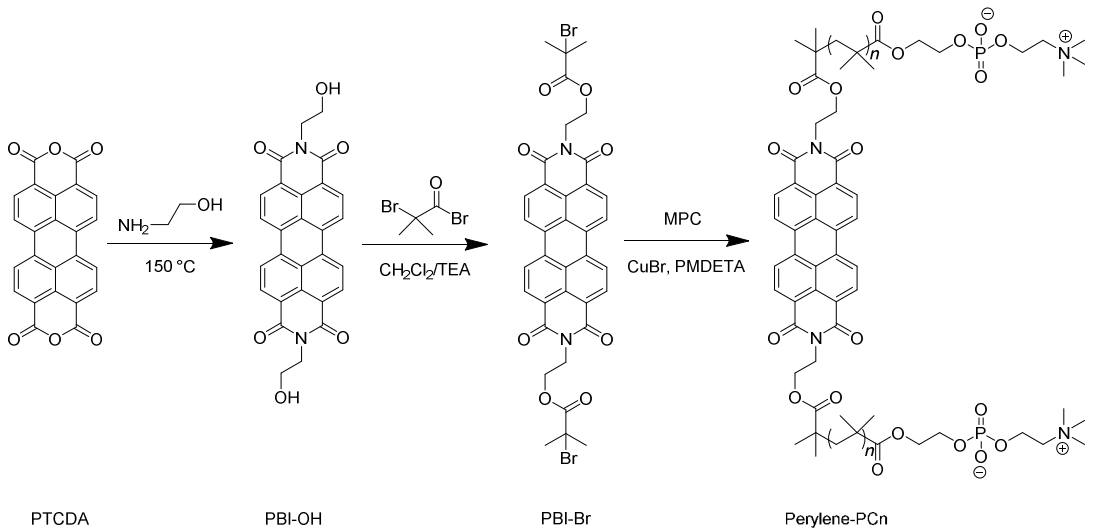

Figure 1. Synthesis routes of Perylene-PCn

View Article Online
DOI: 10.1039/C6RA04349F

Step 2: Preparation of PBI-Br: PBI-OH (430 mg, 1 mmol) was suspended in dry CH_2Cl_2 (150 mL) containing triethylamine (Et_3N, 0.43 mL, 3 mmol). After been cooling to 0 °C, 2-bromoisobutyryl bromide (0.69 g, 3 mmol) in dry CH_2Cl_2 was added dropwise with continuous stirring over a period of 1 h. Then, the reaction mixture was stirred for another 24 h at room temperature. The produced $(CH_3)_3N{\cdot}HBr$ and unreacted PBI-OH were removed by filtration. The target products, PBI-Br remained in CH_2Cl_2 solution was retrieved by drying at 60 °C as dark red solid.

Step 3: Preparation of Perylene-PCn: PBI-Br (40.3 mg, 0.05 mmol), MPC (1 g, 3.4 mmol), CuBr (14.4 mg, 0.01 mmol) and tetrahydrofuran (THF, 15 mL) were introduced into a 25 mL glass flask and the solution was degassed with N_2 for 20 min. After PMDETA (17.3 mg, 0.1 mmol) was added quickly, the flask was sealed and the reactants were kept stirring for 24 h at 60 °C, then the reaction mixture was cooled and filtrated to remove the copper catalyst, followed by drying in a vacuum oven for 24 h [24].

Non-covalent hydrophilization of RGO

In an ice-water bath, 15 mg RGO were dispersed in 20 mL distilled water under an ultrasonic cell disruption system (with power of 600W) for 10 min. After that, 45 mg Perylene-PCn aqueous solutions were added, followed by an additional 10 min ultra-sonication. The mixture was centrifuged at relative centrifugal force (RCF) of 11000 g to obtain the RGO/Perylene-PCn composites. The resultant RGO/Perylene-PCn composites were re-dispersed in ethanol with concentration of 0.5 mg/mL.

Paclitaxel loading on RGO/Perylene-PCn

View Article Online
DOI: 10.1039/C6RA04349F

A series of PTX-ethanol solutions with different concentrations were added to 10 mL RGO/Perylene-PCn solutions. After 30 min sonication, the mixtures were filtered by 0.22 μm membrane to obtain the PTX loading RGO/Perylene-PCn composites, which was recorded as PTX@RGO/Perylene-PCn.

The drug loading content and encapsulation efficiency of PTX loading RGO/Perylene-PCn were analyzed by an Agilent high performance liquid chromatography (HPLC) system with a Zorbax C18 column (150 mm × 4.6 mm, 5 μm, Agilent Technologies, USA). The mobile phase was acetonitrile/water (52/48, v/v). The retention time for PTX was 5.0 min at 227 nm detective wavelength. The drug loading content (DL) was defined as the mass percentage of PTX present in PTX@RGO/Perylene-PCn composites, and encapsulation efficiency (EE) was expressed as the percent of added drug that was entrapped in RGO/Perylene-PCn.

Cell cultivation

HUVEC, RAW264.7, L929 and SG7901 were grown and maintained in DMEM medium supplemented with 15% FBS, 100 μg/mL streptomycin and 100 μg/mL penicillin in a culture flask and were incubated in a 5% CO_2 atmosphere at 37 °C.

Cytotoxicity assay

Viable cells were plated at a density of 5×10^5/mL in 96-well plates and cultivated until the cell monolayer became confluent. RGO/Perylene-PCn was dispersed in cell culture medium by ultrasonication at a concentration of 1 mg/mL. The samples were diluted down to 5 separate concentrations: 10, 25, 50, 75 and 100 μg/mL. According to the drug loading results, PTX loading RGO/Perylene-PCn and free PTX were dispersed in cell culture medium by

View Article Online
DOI: 10.1039/C6RA04349F

ultrasonication at a concentration of 60 μg/mL. Then, the samples were diluted down to 5 separate concentrations: 0.3, 1.5, 3.0, 6.0 and 15.0 μg/mL. A total of 100μL of the dispersions were added to each well and cultured for another 24 h at 37°C. Next, 20 μL of CCK-8 (5 mg/mL in culture medium) was added, and the samples were incubated for another 1 h at 37°C. The absorbance of the solution at 450 nm was recorded with a Rayto RT-6000 microplate reader. Every experiment was performed at least in sextuplicate.

Results and Discussion

Preparation and characterizations of GO and RGO

Firstly, GO and RGO were prepared and FTIR, XRD and XPS were used to characterize the target products. The results were shown in Figure 2. Figure 2A shows the FTIR spectra of graphite, GO and RGO. For GO, oxidation in sulfuric acid provides a typical carboxylic group absorption peak at 1716 cm^{-1} and also provided the absorbance at approximately 1055 cm^{-1}, which corresponds to the other side groups containing C-O bonds such as epoxy, hydroxyl etc. The huge absorption peak at about 3500 cm^{-1} is obviously from the hydroxyl groups. For RGO, most of the side groups on GO have been eliminated in reduction reactions, especially the carboxylate groups. But because the excess usage of hydrazine, which created some defects in the RGO, there are still a few side groups bonded on the GO sheets reflected in FTIR.

Normally, the formation of GO was the result of the expansion of the graphite, which led to the increasing of the inter-lamellar spacing of pristine graphite that could be investigated with XRD. Figure 2B showed the diffraction peaks of pristine graphite, GO and RGO samples.

View Article Online
DOI: 10.1039/C6RA04349F

Compared to the graphite's inter-lamellar spacing of 0.34 nm calculated from Bragg's equation with determined diffraction angle (2θ = 26.4°), GO had a much higher value of 0.78 nm (2θ = 12.3°), due to the formation of oxygen-containing function groups on carbon basal planes. The result agreed with the literatures and proved the successful preparation of GO [41, 42]. After being reduced by Hydrazine Hydrate, the incisive peak of GO disappeared, a weak and broad peak appeared at 2θ = 24.2°, indicating the restack of graphene sheets.

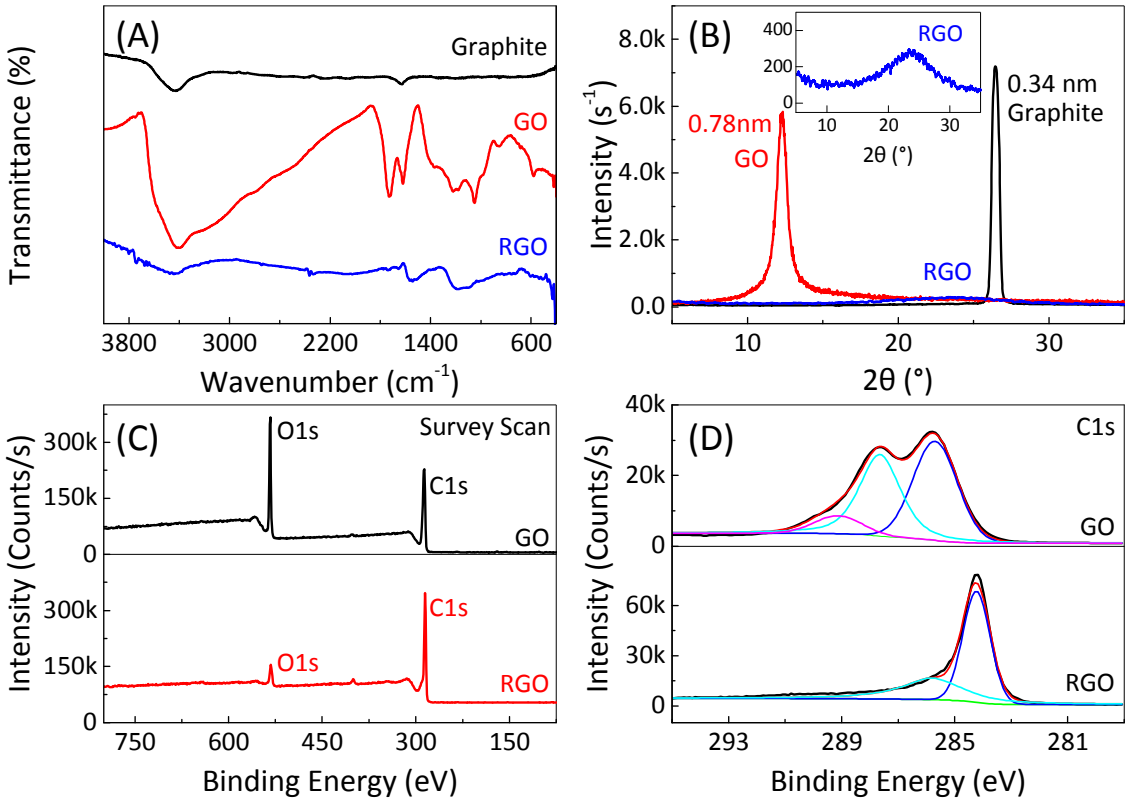

Figure 2. Spectrum characterization of GO and RGO. Where (A), FTIR; (B), XRD of graphite, GO and RGO; (C), XPS survey scan of GO and RGO; and (D), XPS intensive scan for C1s of GO and RGO

The XPS survey scan and C1s spectra of GO nanosheets were shown in Figure 2C and 1D. The C1s spectrum of GO sheets can be fitted with three peak composites with binding energies

View Article Online
DOI: 10.1039/C6RA04349F

at about 284.8, 286.6 and 289.0 eV, attributable to the C-C, C-O and O-C=O species, respectively [43]. Figure 2C also showed the survey scan spectra of RGO nanosheets from chemical reducing. Comparing to the spectra of the GO nanosheets, the O1s signal of RGO nanosheets at the binding energy of about 533eV decreased significantly, suggesting that most of the oxygen-containing functionalities in GO have been reduced or removed. The XPS C1s spectrum of the RGO nanosheets (Figure 2D) can be curve-fitted into two peak components with binding energies at about 284.2 and 285.7eV, which belongs to the C-C and C-N species, respectively [43].

Chemical, physical and endocytosis properties of synthesized Perylene-PCn

Figure 3A shows the FTIR spectra of PTCDA and Perylene-PC. The spectra of the PTCDA used by us is fully compatible with the standard spectra in HR Aldrich FTIR collection Edition II (Spectra No. 11350). On the Perylene-PCn curve, the peak at 3400 cm^{-1} corresponds to the hydroxyl group (-OH), while the double peaks at 3034 and 2956 cm^{-1} are associated with the transformation of the methylene carbon. The absorbance at 964 cm^{-1} was assigned to a tertiary amine group while the peak at approximately 1247 cm^{-1} is due to the synergistic effect of the phosphate and the tertiary amine groups; the peak at 1489 cm^{-1} belongs to the P-O-alkyl and the amide groups [44].

The ^{1}H-NMR spectra of Perylene-PCn in D_2O was shown in Figure 3B. The incisive peak at 4.70 ppm is the resonance of H_2O. The chemical shifts in the ranges of 0.86, 1.05 and 1.11 ppm belong to the methyl protons of the MPC and 2-bromoisobutyryl bromide, respectively. The peak at 3.20 ppm is the methyl protons of the quaternary amine that comes from

View Article Online
DOI: 10.1039/C6RA04349F

phosphorylcholine. The typical signals of Perylene at 8.0-8.5 ppm persist in the polymer products, indicating that the Perylene moieties have been successfully attached to the polymers. The number-average molecule weight of oligomeric PCn was determined by integrating the area of peaks at 3.20 ppm and 8.0-8.5 ppm. Using the methyl protons of the quaternary amine and protons on perylene core as the standards, the degree of polymerization n is about 32, indicating that the number-average molecular weight is about 9800 g/mol.

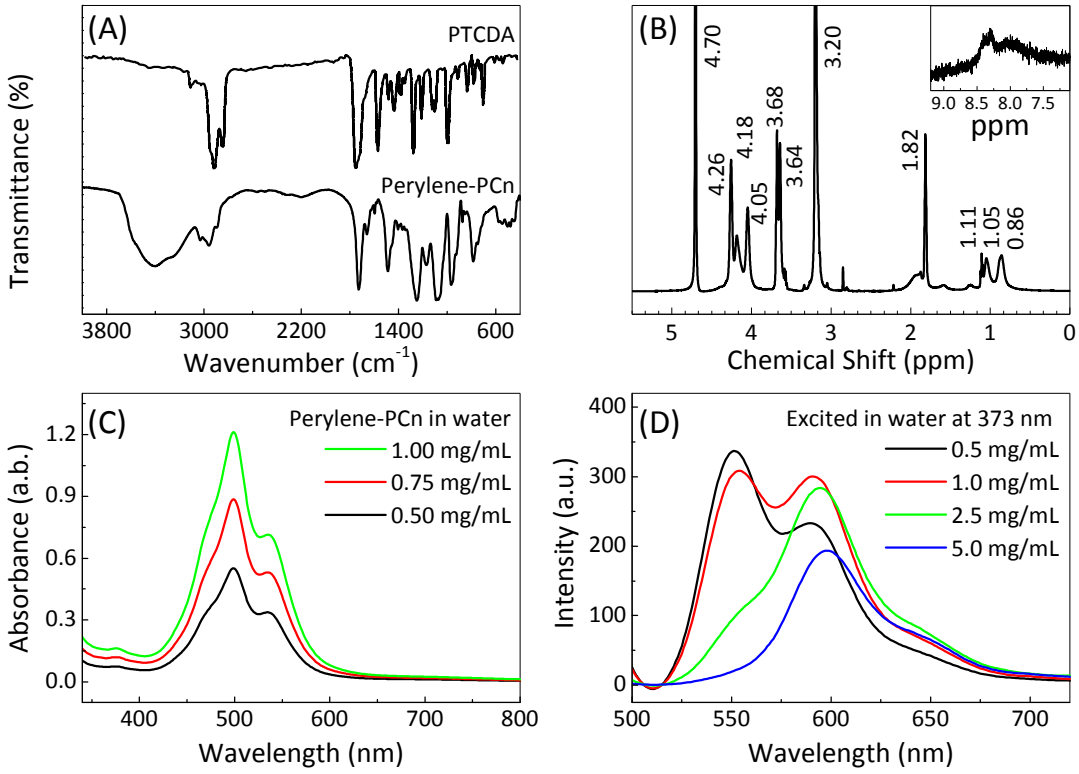

Figure 3. Characterizations of Perylene-PCn. Where (A). FTIR; (B). ^{1}H-NMR spectra of Perylene-PCn; (C). UV-Visible spectra; and (D). fluorescence excitation spectra of Perylene-PCn in water

The optical properties of Perylene-PCn were investigated by UV-visible absorption spectra

View Article Online
DOI: 10.1039/C6RA04349F

and fluorescence spectroscopy, as shown in Figure 3C. Three different concentrations of Perylene-PCn water solution were investigated by UV-visible absorption, including 0.50, 0.75 and 1.00 mg/mL. The UV-visible absorption spectrum of Perylene-PCn in H_2O shows the presence of three adsorption bands at 475, 501 and 543 nm, corresponding to the 0→2, 0→1 and 0→0 electronic transitions of perylene moiety [45]. The maximum absorption is at the wavelength of 501 nm which is the $\lambda_{0\text{-}1}$ vibration band, whereas the $\lambda_{0\text{-}0}$ adsorption band at 543 nm is relatively weak, suggesting that Perylene-PCn aggregates in water to some degrees. Obviously, the absorption is also related to the concentration itself, which increased with the increasing of concentration. By using the Beer-Lambert law ($A=\varepsilon lC$), the molar absorption coefficient of Perylene-PCn at 501 nm can be calculated as 11418 $L\cdot mol^{-1}\cdot cm^{-1}$.

The concentration-dependent fluorescence behavior of the Perylene-PCn in water at the excitation wavelength λ_{ex} = 373 nm was also investigated and the results were shown in Figure 3D. The photo luminescent properties of perylene was retained in Perylene-PCn. A well-resolved vibronic pattern was shown. The fluorescence intensity and the patterns of Perylene-PCn in aqueous solution varied a lot at different concentrations, due to the self-quenching of perylene dye at high concentration. At the concentration of 5.0 mg/mL, the fluorescence intensity was less than 200 a.u. and showed single fluorescence wavelength at about 600 nm. When the concentration was diluted to 2.5 mg/mL, the fluorescence intensity at 600 nm became stronger and a weak fluorescence-emission appeared at about 550 nm. By further diluting the concentration to 1.0 mg/mL, two fluorescence-emission bands with nearly equal intensity presented and both of the bands were stronger than the ones observed at higher concentration. By even diluting the

View Article Online
DOI: 10.1039/C6RA04349F

concentration further to 0.5 mg/mL, the emission at about 550 nm was even stronger than that at 600 nm and the fluorescence excitation band showed obvious red shifting, which was similar to the previous reports [24].

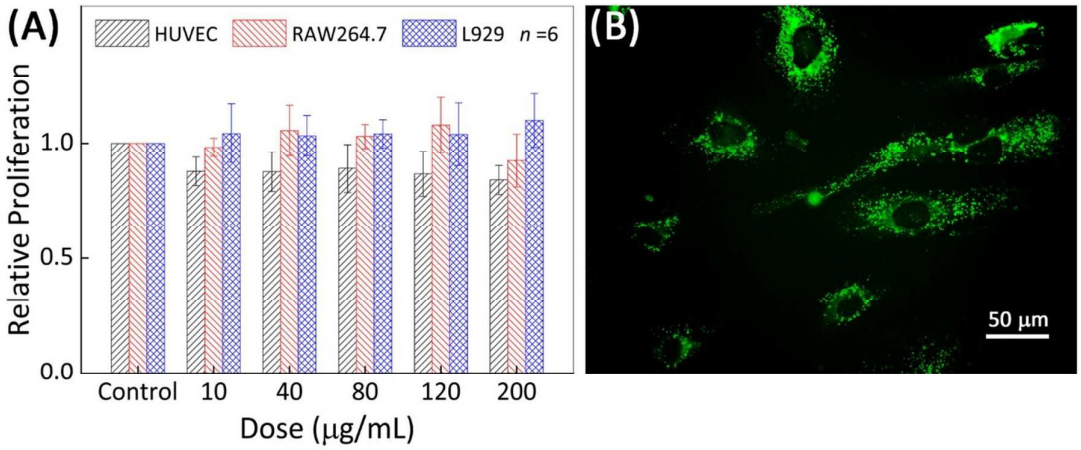

Figure 4. Cytotoxicity assay (A) and confocal fluorescent image of endocytosis of Perylene-PCn in HUVECs (B)

The *in vitro* cytotoxicity of Perylene-PCn were investigated to evaluate its biomedical applications. The studies were performed against three different cell lines, HUVEC, RAW264.7 and L929 at a series of concentrations for 24 h. The results were shown in Figure 4A. The relative cell proliferations data were determined by CCK-8.

Among the three different cell lines, after exposure to Perylene-PCn HUVECs showed relatively lower extent of proliferation than that of L929 and RAW264.7. However, comparing to the blank control group, even after raising the Perylene-PCn concentrations from 10 μg/mL to 200 μg/mL, the relative proliferations of all three cells exposure to Perylene-PCn remained higher than 80% and show no statistical difference. The results suggest that HUVEC is the most sensitive cell lines among the three studied here to the

View Article Online
DOI: 10.1039/C6RA04349F

exotic substance, but even for HUVEs Perylene-PCn showed very low cytotoxicity after a 24-hour exposure.

As shown in Figure 3D, Perylene-PCn was presented with a high photoluminescence quantum yield with recognizable green fluorescence, therefore can be potentially used as a fluorescent probe. Based on this observations, we investigated the fluorescent images of HUVECs exposure to Perylene-PCn for 24 h with a confocal microscopy. A typical photograph was shown in Figure 4B. As shown in Figure 4B, Perylene-PCn permeated through the cell membrane and distributed in cytoplasm, emitting intensive green fluorescence. However, in the nucleus, no fluorescence was observed, which indicated that Perylene-PCn cannot enter cell nucleus because of its macromolecular properties.

Non-covalent hydrophilization of RGO with Perylene-PCn

Figure 5A shows the Raman spectra of graphite, GO, RGO and RGO/Perylene-PCn composites, which was roughly identical with the previous report [46]. In the Raman spectra, the original graphite has a weak D band at 1350 cm^{-1} and an incisive G band at 1580 cm^{-1} [47]. However, The D band of GO and RGO increased significantly. In addition, the G band shifted to higher frequencies due to graphite amorphization. Both of the observations confirmed the lattice distortions caused by oxidation and reduction processes. Furthermore, the 2D band at 2700 cm^{-1} is highly sensitive to stacking of graphene sheets [48]. The Raman spectrum of graphite shows an incisive band relating to its multilayer structure. After oxidation and reduction, GO and RGO showed an decreased and broadened peak at around 2700 cm^{-1}, which indicated a mixed single and few-layer structure [48]. The new peak at about 2940 cm^{-1}

View Article Online
DOI: 10.1039/C6RA04349F

(D+G) also proved the disorder-induced combination mode [49]. Moreover, The GO layers will agglomerate while using excess amount of hydrazine and creates defects in the RGO. Raman spectra of RGO showed that the defect content in RGO is increased as compared to GO. The sp3 hybridization of GO should change to sp2 in the RGO resulting lower defects. However, the present data shows that the defect in RGO is higher as compared to GO. It may be attributed to the use of excess hydrazine[37]. After been compounded with Perylene-PCn, the D band of RGO at 1350 cm^{-1} transformed to a double peak at 1290 and 1369 cm^{-1}, which indicated the further disordering of carbon bonds in the composite caused by the introduction of Perylene-PCn polymeric structures. The changes in Raman spectra proved the successfully synthesis and preparation of RGO/Perylene-PCn composites.

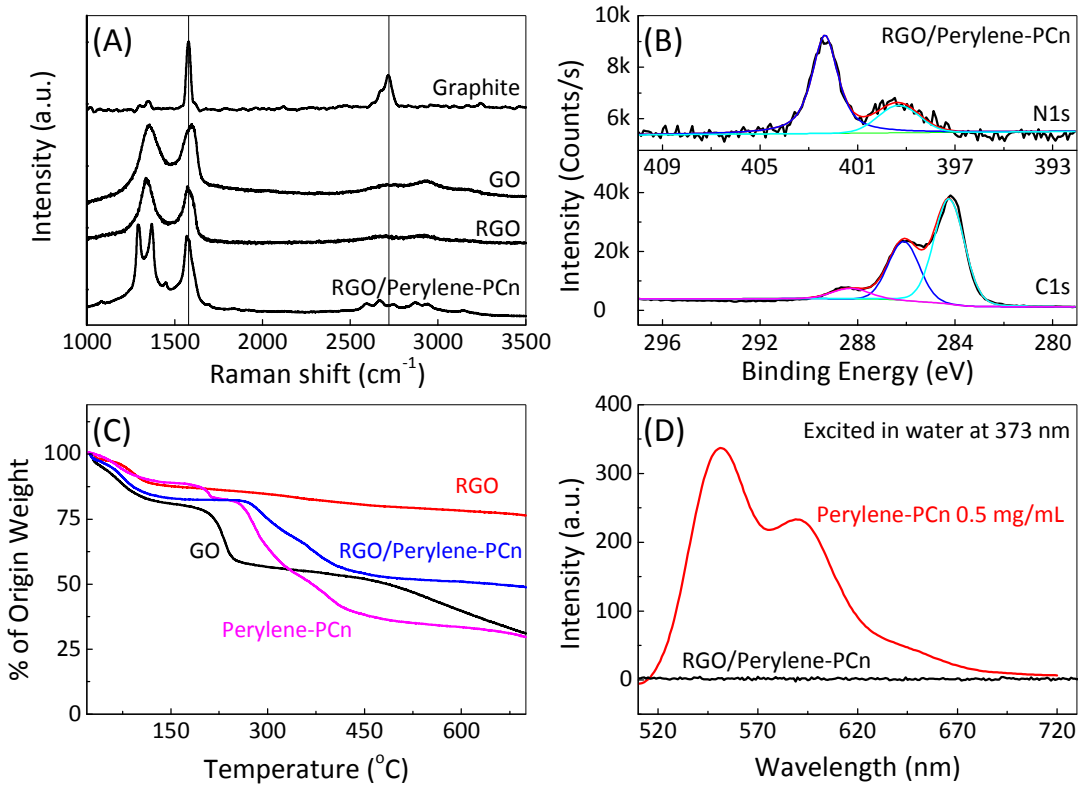

Figure 5. Characterizations of RGO/Perylene-PCn composites. Where (A). Raman spectra; (B).

View Article Online
DOI: 10.1039/C6RA04349F

XPS intensive scanning of C and N in RGO/Perylene-PCn; (C). TGA analysis; and (D). Fluorescent spectra of composite and its compositions.

As shown in Figure 5B, the XPS C1s spectrum of the resulting RGO/Perylene-PCn composites could be curve-fitted into three peak components with binding energies at 284.2, 286.0 and 288.7eV, attributable to the C-C, C-O/C-N and O-C=O species, respectively. The increase in relative intensity of the C-O peak component and the appearance of the C-N peak component comparing to RGO XPS spectra shown in Figure 2D, and N1s signal shown in Figure 5B were consistent with the successful composition of RGO and Perylene-PCn. The XPS N1s core-level spectrum of the resulting RGO/Perylene-PCn composites could be curve-fitted into two major peak components with binding energies at about 399.4 and 402.3 eV, attributable to the bisimide group and the quaternary amine species, indicating that both phosphorylcholine groups and perylene bisimide core were introduced.

Figure 5C shows the TGA curves of GO, RGO, Perylene-PCn and RGO/Perylene-PCn composites at a heating rate of 20 °C/min in nitrogen atmosphere. For GO, the 12% weight loss below 120 °C should due to the evaporation of the residual adsorbed and combined water which occupied the spaces between the GO layers. By continuing heating up to 300 °C, the labile oxygen-containing functional groups decomposed gradually. The fasted decomposition temperature was recorded at about 220 °C, at which about 30% weight loss was observed. After that, the slowly weight loss was due to the decomposition of the carbon backbone which continued until 700 °C, when 30% mass remained. RGO exhibited better thermal stability. It was stable over a wide temperature range, with only about 10% mass lost due to the removal of the residual water at temperature below 120 °C and only about 5%

View Article Online
DOI: 10.1039/C6RA04349F

mass lost beyond 120 °C in a wide temperature range due to the decomposition of the residual oxygen functional groups. The TGA curve of the RGO/Perylene-PCn composites showed a major weight loss between 300-400 °C due to the decomposition of Perylene-PCn, which was consistent with the decomposition of Perylene-PCn itself as shown on the TG curve. The consistency indicated that the interaction of RGO and Perylene-PCn was π-π stacking rather than covalence bonds. The main residual component in the RGO/Perylene-PCn composites at 700 °C was RGO with a weight content of 50%, indicating that the ratio of RGO to Perylene-PCn was about 5:2.

The fluorescence spectrum of the RGO/Perylene-PCn composites in water obtained at an excitation wavelength λ_{ex}=373 nm was shown in Figure 5D. The fluorescence emission of the RGO/Perylene-PCn composites was completely quenched due to the charge or energy transfer, consistent with the presence of strong π-π stacking interactions between the perylene moieties and the RGO nanosheets.

View Article Online
DOI: 10.1039/C6RA04349F

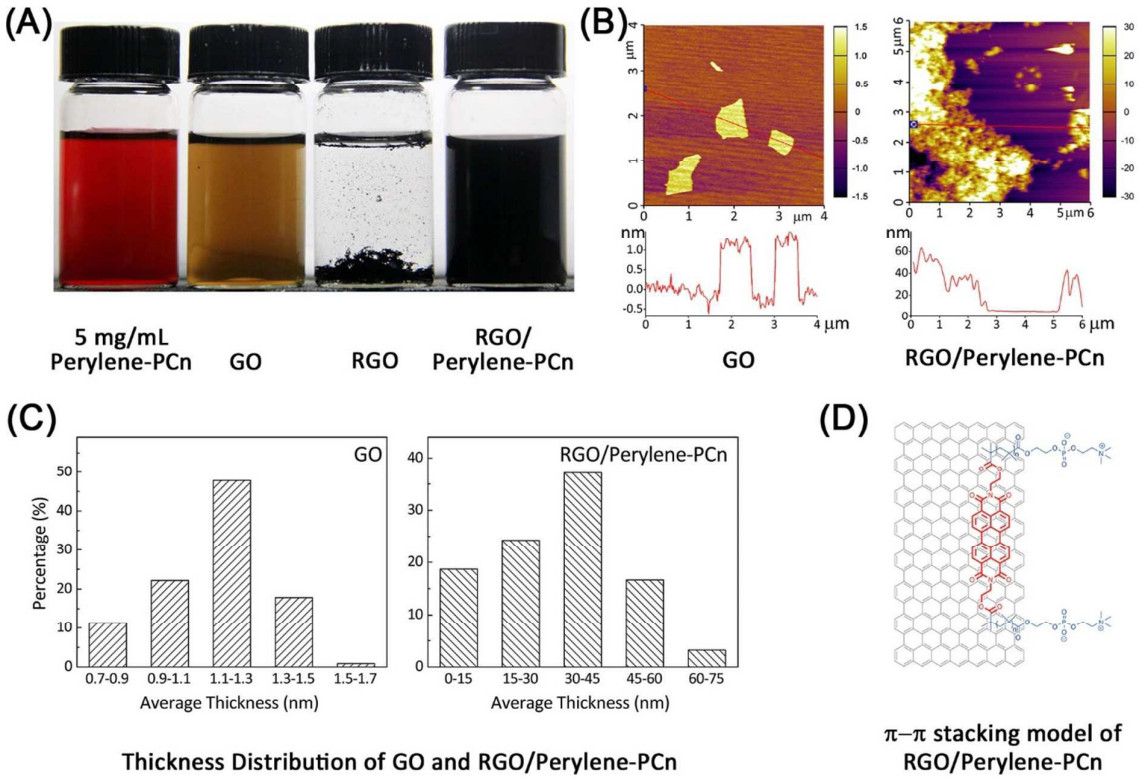

Figure 6. Water dispersion photographs (A), AFM images (B), Thickness distribution in AFM (C), and π–π stacking model (D) of RGO/Perylene-PCn composite.

Figure 6A shows the photographic images of aqueous dispersions of Perylene-PCn, GO, RGO, and RGO/Perylene-PCn. With modifications by the water-soluble poly(2-methacryloyloxyethyl phosphorylcholine) segments, the insoluble PTCDA dissolved in water homogenously. GO was also presented as a pseudo-homogeneous yellow-brown dispersion for the hydrophilic oxygen containing groups' modification, but RGO completely precipitated after been reduced. In the RGO/Perylene-PCn system, it was obvious that RGO was solubilized by Perylene-PCn. The RGO/Perylene-PCn composites remained stable and uniformly dispersed in the aqueous solution for at least three days, indicating the successful π-π stacking interaction between RGO nanosheets and perylene core.

View Article Online
DOI: 10.1039/C6RA04349F

The AFM images of GO and RGO/Perylene-PCn, as shown in Figure 6B, further confirmed the interaction between RGO sheets and Perylene core. The original GO sheets that were spin-coated on a mica substrate showed an ultra-flat like slice, had smooth edges and had a thickness of 1.0 nm. For the samples of RGO/Perylene-PCn, due to the agglomeration and the attachment of Perylene-PCn onto RGO surface, the surface became rough and had various bulges with average heights of 40 nm. Some ultra-flat sheets with a thickness of 1.0 nm were also seen in the images, indicating that some surface was not covered by Perylene-PCn. Figure 6C shows the AFM thickness distribution of GO and RGO/Perylene-PCn composites studied at different areas of the substrates. It shows that the thickness of ~70% of GO sheets is in the 0.9-1.3 nm range and the thickness of ~18% of GO sheets is in the 1.3-1.5 nm range. After being composed as RGO/Perylene-PCn, the thickness of ~78% of composites is in the 15-60 nm thickness. Thus, few layer graphene sheets were formed during the synthesis of GO, while most of the RGO sheets become much more thick because of the agglomeration and the covering by Perylene-PCn.

In summary, RGO interacted with Perylene-PCn through π-π stacking as shown in Figure 6D. As for GO, after been reduced by hydrazine, most of the oxygen containing groups on graphene nanosheets were removed and their blocking effects no longer exist, the graphene nanosheets then tended to restack due to the strong Van de Waals force. When Perylene-PCn solution was added into the RGO dispersion, with a slight ultrasonic treatment, the perylene core was attached to RGO surface through π-π stacking interaction. Once enough Perylene-PCn attached onto the RGO nanosheets, due to the excellent water solubility of PCn segments, the RGO/Perylene-PCn formed a stable dispersion in water again.

View Article Online
DOI: 10.1039/C6RA04349F

Paclitaxel loading on RGO/Perylene-PCn

Figure 7A shows the FTIR spectra of PTX, RGO/Perylene-PCn composites and PTX loaded RGO/Perylene-PCn composites (PTX@RGO/Perylene-PCn). Several characteristic FTIR absorption peaks of PTX appeared in the spectra of PTX@RGO/Perylene-PCn, including the broad absorption at 3400-3500 cm^{-1}, the enhanced peak at 1720 cm^{-1} related to the combination of carbonyl groups which exist in both PTX and RGO/Perylene-PCn, the peak at 1650 cm^{-1} related to the amido linkage in PTX molecule, and the peak at 712 cm^{-1} related to the mono-substituted benzene structure in PTX. The result indicated the successful loading of PTX on RGO/Perylene-PCn.

The PTX loading content and encapsulation efficiency were assessed by HPLC. As shown in Figure 7B, the drug loading content increased with the increasing of weight ratio of PTX to RGO/Perylene-PCn, and reached as high as about 25% at the ratio of 3. Considering both the economic aspect and efficiency, to add 1 equivalent of PTX to 1 equivalent of RGO/Perylene-PCn composites should be the best choice. The loading capacity of PTX on RGO/Perylene PCn is about 15% at this ratio.

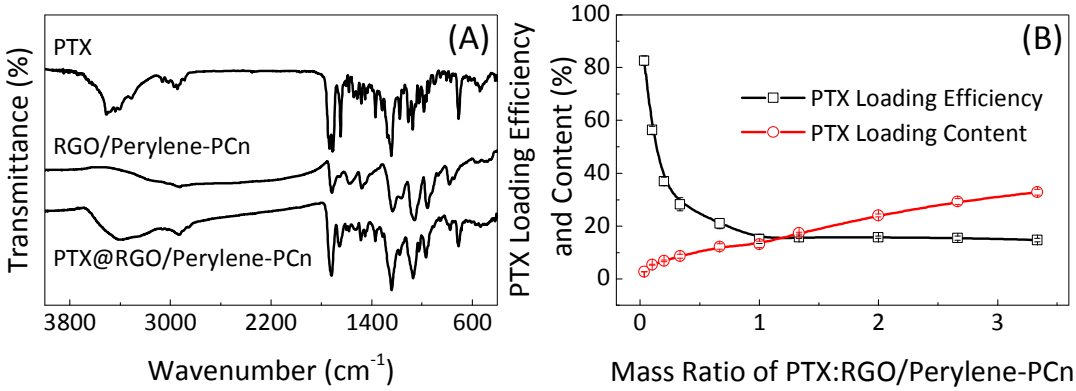

Figure 7. (A). FTIR of PTX, RGO/Perylene-PCn and PTX@RGO/Perylene-PCn; (B). Drug loading

View Article Online
DOI: 10.1039/C6RA04349F

efficiency and contents of PTX on RGO/Perylene-PCn composites

Cytotoxicity assay of RGO/Perylene-PCn, PTX and PTX@RGO/Perylene-PCn

In our previous work, we demonstrated that GO showed cytotoxicity with a dose dependent manner. Because of the huge specific surface area and hydrophobic conjugated aromatic structure of GO, many cell membrane biomolecules, such as peptides, proteins, polysaccharides and other molecules with hydrophobic moiety can be attracted and adsorbed by GO sheets, which in turn wrapped the cells by aggregation and then affected the normal function of cell membrane[44]. After covering the RGO surface with Perylene-PCn, it was highly likely that the surface of RGO/Perylene-PCn was covered by hydrophilic phosphorylcholine oligomer which hindered the interaction between the conjugated aromatic structure and cell membrane molecules, thus improve the biocompatibility of RGO/Perylene-PCn. In order to verify the reduction in cytotoxicity and also to evaluate the anti-tumor efficiency of PTX@RGO/Perylene-PCn system, *in vitro* cytotoxicity assays were carried out and the results were shown in Figure 8.

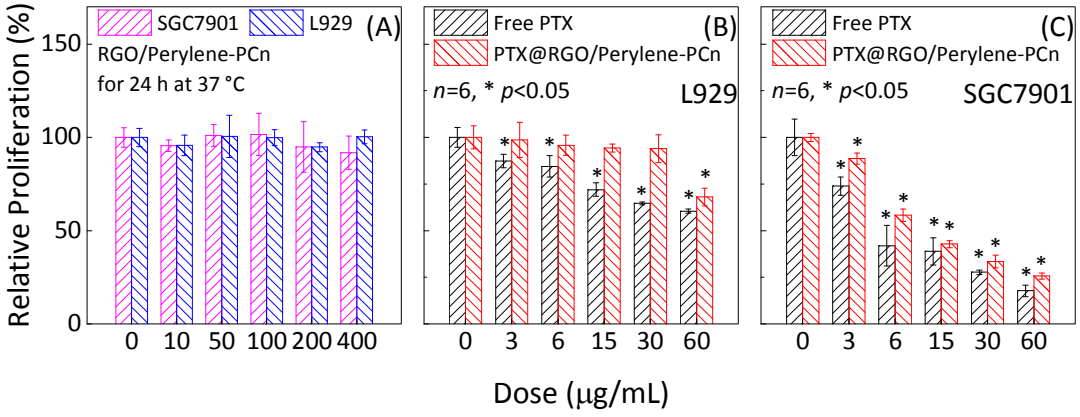

Figure 8. Cytotoxicity assay of RGO/Perylene-PCn, PTX and PTX@RGO/Perylene-PCn. Where A. Cell compatibility assay of RGO/Perylene-PCn against L929 and SGC1901 cells; B. L929

View Article Online
DOI: 10.1039/C6RA04349F

cytotoxicity of free PTX and PTX@RGO/Perylene-PCn; and C. anti-tumor comparison of free PTX and PTX@RGO/Perylene-PCn using SGC7901 as model cells.

Figure 8A shows the relative cell proliferation of SGC7901 and L929 cell lines after being exposed to RGO/Perylene-PCn composites for 24 h at the dosages ranged from 10 to 400 μg/mL. Under all of the doses, both cell lines proliferated well and the relative cell proliferations showed no statistical differences comparing to the control group, proving the good cell-compatibility of RGO/Perylene-PCn composites.

The *in vitro* cytotoxicity of PTX@RGO/Perylene-PCn was further evaluate using SGC7901 cell line. L929 was used as a comparison. The result indicated the anti-tumor properties. Figure 8B and 7C shows the relative proliferations of two cell lines after being exposed to PTX and the PTX@RGO/Perylene-PCn for 24 h. The dose range was 10 to 60 μg/mL. In PTX@RGO/Perylene-PCn, the dosage was calculated as the loaded free PTX (with PTX content 15%). For L929 cell lines, the exposure to free PTX led to significant cell cytotoxicity, even at the lowest dose of 3 μg/mL. However, as the dose was raised, the cell apoptosis did not increase accordingly. After PTX was loaded onto RGO/Perylene-PCn, cytotoxicity can only be observed at the concentration as high as 60 μg/mL. For SGC7901, a typical gastric carcinoma cell line, the introduction of PTX inhibited the cell proliferation remarkably. With a low PTX concentration of 6 μg/mL, the relative cell proliferation was reduced to less than 50%. A dose dependence decreasing was observed. The same trend was also observed in the assay of SGC7901 being exposed to PTX@RGO/Perylene-PCn, but relatively higher proliferation was observed. The result suggested that the wrap of PTX by RGO/Perylene-PCn could reduce the cytotoxicity of free PTX. It is beneficial for the situations where the

View Article Online
DOI: 10.1039/C6RA04349F

reduction of the side effect of PTX is necessary.

Conclusions

A water-soluble and biocompatible Perylene-PCn was synthesized by a typical ATRP procedure, while GO and RGO was prepared according to Hummer's method. RGO/Perylene-PCn composite was fabricated through π-π stacking interactions between RGO and Perylene moiety. The properties of the composites were extensively investigated and the structures were proved. Furthermore, PTX was successfully loaded in RGO/Perylene-PCn. Using the typical tumor cell line SGC7901 as a model system, the *in vitro* cytotoxicity assay of PTX@RGO/Perylene-PCn presented the similar anti-tumor efficacy comparing to free PTX. The results highlighted RGO/Perylene-PCn as an anti-tumor agent delivery vehicle for potential oncology applications.

Acknowledgements

The authors acknowledge the support of Science and Technology Support Program (Society Development) of Jiangsu Province (No. BE2012735), the National Basic Research Program of China (No. 2011CB933400), the Foundation of Jiangsu Provincial Key Laboratory for Interventional Medical Devices (No. JR1504). The works are also a part of the Project Funded by the Priority Academic Program Development of Jiangsu Higher Education Institutions (PAPD).

References

1. K. S. Novoselov, A. K. Geim, S. V. Morozov, D. Jiang, M. I. Katsnelson, I. V. Grigorieva, S. V. Dubonos and A. A. Firsov, *Nature*, 2005, 438, 197-200.
2. Y. Zhang, Y. W. Tan, H. L. Stormer and P. Kim, *Nature*, 2005, 438, 201-204.

View Article Online
DOI: 10.1039/C6RA04349F

3. A. K. Geim and K. S. Novoselov, *Nat Mater*, 2007, 6, 183-191.
4. J. C. Meyer, A. K. Geim, M. I. Katsnelson, K. S. Novoselov, T. J. Booth and S. Roth, *Nature*, 2007, 446, 60-63.
5. Y. Wang, Z. Li, J. Wang, J. Li and Y. Lin, *Trends Biotechnol*, 2011, 29, 205-212.
6. L. Feng, L. Wu and X. Qu, *Adv Mater*, 2013, 25, 168-186.
7. G. Goncalves, M. Vila, M. T. Portoles, M. Vallet-Regi, J. Gracio and P. A. A. P. Marques, *Advanced Healthcare Materials*, 2013, 2, 1072-1090.
8. K. Yang, L. Feng, X. Shi and Z. Liu, *Chem Soc Rev*, 2013, 42, 530-547.
9. H. Shen, L. Zhang, M. Liu and Z. Zhang, *Theranostics*, 2012, 2, 283-294.
10. L. Feng and Z. Liu, *Nanomedicine (Lond)*, 2011, 6, 317-324.
11. Y. Pan, N. G. Sahoo and L. Li, *Expert Opin Drug Deliv*, 2012, 9, 1365-1376.
12. Z. Liu, J. T. Robinson, S. M. Tabakman, K. Yang and H. Dai, *Materials Today*, 2011, 14, 316-323.
13. D. Ghosh, S. Chandra, A. Chakraborty, S. K. Ghosh and P. Pramanik, *Int J Pharm Sci Drug Res*, 2010, 2, 127-133.
14. L. J. Cote, F. Kim and J. Huang, *J Am Chem Soc*, 2009, 131, 1043-1049.
15. D. Li, M. B. Muller, S. Gilje, R. B. Kaner and G. G. Wallace, *Nat Nanotechnol*, 2008, 3, 101-105.
16. S. Niyogi, E. Bekyarova, M. E. Itkis, J. L. McWilliams, M. A. Hamon and R. C. Haddon, *J Am Chem Soc*, 2006, 128, 7720-7721.
17. Y. Si and E. T. Samulski, *Nano Lett*, 2008, 8, 1679-1682.
18. S. Stankovich, R. D. Piner, X. Q. Chen, N. Q. Wu, S. T. Nguyen and R. S. Ruoff, *Journal of Materials Chemistry*, 2006, 16, 155-158.
19. J. Liu, L. Tao, W. Yang, D. Li, C. Boyer, R. Wuhrer, F. Braet and T. P. Davis, *Langmuir*, 2010, 26, 10068-10075.
20. J. Q. Liu, W. R. Yang, L. Tao, D. Li, C. Boyer and T. P. Davis, *J Polym Sci Pol Chem*, 2010, 48, 425-433.
21. L. Feng, S. Zhang and Z. Liu, *Nanoscale*, 2011, 3, 1252-1257.
22. Y. Yang, Y. M. Zhang, Y. Chen, D. Zhao, J. T. Chen and Y. Liu, *Chemistry-a European Journal*, 2012, 18, 4208-4215.
23. D. Depan, J. Shah and R. D. K. Misra, *Mat Sci Eng C-Mater*, 2011, 31, 1305-1312.
24. L. Q. Xu, L. Wang, B. Zhang, C. H. Lim, Y. Chen, K. G. Neoh, E. T. Kang and G. D. Fu, *Polymer*, 2011, 52, 2376-2383.
25. W. Feng, S. Zhu, K. Ishihara and J. L. Brash, *Langmuir*, 2005, 21, 5980-5987.
26. D. Chapman, *Langmuir*, 1993, 9, 39-45.
27. K. Ishihara, T. Ueda and N. Nakabayashi, *Polymer Journal*, 1990, 22, 355-360.
28. H. H. Hub, B. Hupfer, H. Koch and H. Ringsdorf, *Angew Chem Int Edit*, 1980, 19, 938-940.
29. K. Ishihara, H. Nomura, T. Mihara, K. Kurita, Y. Iwasaki and N. Nakabayashi, *Journal of biomedical materials research*, 1998, 39, 323-330.
30. K. Ishihara, H. Oshida, Y. Endo, A. Watanabe, T. Ueda and N. Nakabayashi, *J Biomed Mater Res*, 1993, 27, 1309-1314.
31. J. A. Hayward and D. Chapman, *Biomaterials*, 1984, 5, 135-142.
32. A. L. Lewis, Z. L. Cumming, H. H. Goreish, L. C. Kirkwood, L. A. Tolhurst and P. W. Stratford, *Biomaterials*, 2001, 22, 99-111.
33. Y. Iwasaki, S. Sawada, K. Ishihara, G. Khang and H. B. Lee, *Biomaterials*, 2002, 23, 3897-3903.
34. T. Zhang, K. Xi, M. Gu and Z. S. Jiang, *Chinese Chemical Letters*, 2008, 19, 105-109.
35. J. Sakamoto, T. Matsui and Y. Kodera, *Gastric Cancer*, 2009, 12, 69-78.

View Article Online
DOI: 10.1039/C6RA04349F

36. W. S. Hummers Jr and R. E. Offeman, *J Am Chem Soc*, 1958, 80, 1339-1339.
37. S. Stankovich, D. A. Dikin, R. D. Piner, K. A. Kohlhaas, A. Kleinhammes, Y. Jia, Y. Wu, S. T. Nguyen and R. S. Ruoff, *Carbon*, 2007, 45, 1558-1565.
38. Y. Xu, H. Bai, G. Lu, C. Li and G. Shi, *J Am Chem Soc*, 2008, 130, 5856-5857.
39. A. V. Ustinov, V. V. Dubnyakova and V. A. Korshun, *Tetrahedron*, 2008, 64, 1467-1473.
40. A. V. Ustinov, V. V. Dubnyakova and V. A. Korshun, *Nucleosides Nucleotides Nucleic Acids*, 2007, 26, 751-754.
41. Y. Matsuo, K. Tahara and Y. Sugie, *Carbon*, 1997, 35, 113-120.
42. J. Q. Wang and Z. D. Han, *Polymers for Advanced Technologies*, 2006, 17, 335-340.
43. L. Q. Xu, W. J. Yang, K. G. Neoh, E. T. Kang and G. D. Fu, *Macromolecules*, 2010, 43, 8336-8339.
44. Y. Liu, Y. Zhang, T. Zhang, Y. J. Jiang and X. F. Liu, *Carbon*, 2014, 71, 166-175.
45. H. M. Liu, Y. L. Wang, C. H. Liu, H. X. Li, B. X. Gao, L. C. Zhang, F. L. Bo, Q. Q. Bai and X. W. Ba, *Journal of Materials Chemistry*, 2012, 22, 6176-6181.
46. D. C. Marcano, D. V. Kosynkin, J. M. Berlin, A. Sinitskii, Z. Sun, A. Slesarev, L. B. Alemany, W. Lu and J. M. Tour, *ACS Nano*, 2010, 4, 4806-4814.
47. I. Calizo, A. A. Balandin, W. Bao, F. Miao and C. N. Lau, *Nano Lett*, 2007, 7, 2645-2649.
48. A. C. Ferrari, J. C. Meyer, V. Scardaci, C. Casiraghi, M. Lazzeri, F. Mauri, S. Piscanec, D. Jiang, K. S. Novoselov, S. Roth and A. K. Geim, *Phys Rev Lett*, 2006, 97, 187401.
49. J. Campos-Delgado, J. M. Romo-Herrera, X. Jia, D. A. Cullen, H. Muramatsu, Y. A. Kim, T. Hayashi, Z. Ren, D. J. Smith, Y. Okuno, T. Ohba, H. Kanoh, K. Kaneko, M. Endo, H. Terrones, M. S. Dresselhaus and M. Terrones, *Nano Lett*, 2008, 8, 2773-2778.

View Article Online
DOI: 10.1039/C6RA04349F

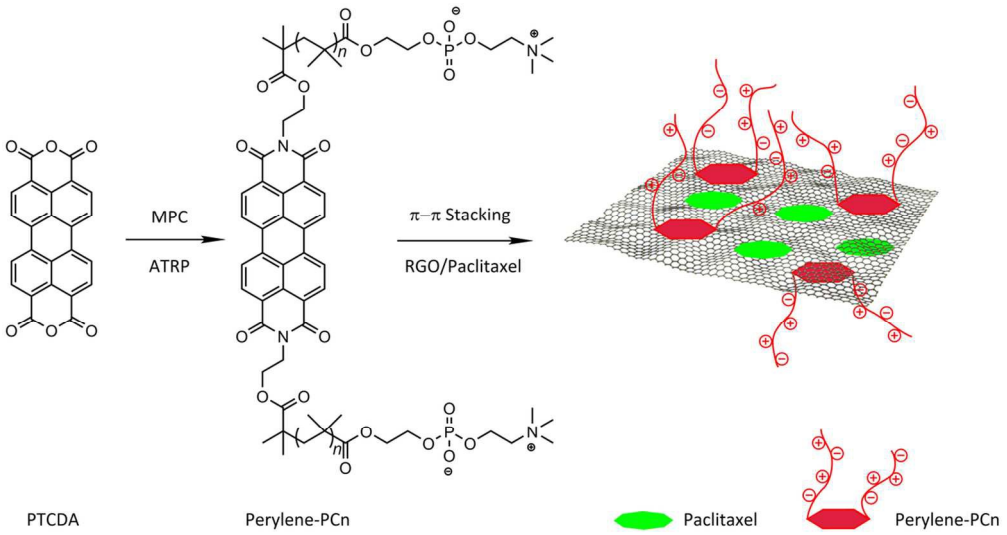

116x61mm (300 x 300 DPI)